journal

J. Am. Ceram. Soc., **88** [8] 2236–2245 (2005)
DOI: 10.1111/j.1551-2916.2005.00434.x

Effects of Moisture on Grain-Boundary Strength, Fracture, and Fatigue Properties of Alumina

J. J. Kruzic,*,† R. M. Cannon,** and R. O. Ritchie*,‡

Materials Sciences Division, Lawrence Berkeley National Laboratory, and Department of Materials Science and Engineering University of California, Berkeley California 94720

The role of moisture in affecting both intrinsic and extrinsic aspects of the fracture and fatigue-crack growth resistance of a polycrystalline alumina (99.5% pure, 25 μm grain size) has been examined in both moist and dry environments at ambient temperature. The intrinsic (crack-tip) toughness, deduced from measured crack-opening profiles, is found to be less than for a single crystal and is 30% lower ($\sim$0.6 MPa·m$^{1/2}$) in moist air versus in dry N_2, implying that the grain-boundary theoretical strength is higher in a dry environment. Despite this, in dry atmospheres, the *R*-curves (which derive from crack deflection and grain bridging) initially rose more steeply and nominal fatigue-crack growth thresholds for short crack sizes (20–60 μm) were more than 1.3 MPa·m$^{1/2}$ higher. Owing to this quicker crack bridging development, strengths for natural flaws could be more than doubled in dry atmospheres, a difference that well exceeds the effect solely due to the intrinsic toughness change. After $\sim$2 mm of crack growth, however, the *R*-curve and steady-state fatigue behavior appeared similar in both environments, although altering the atmosphere for such fatigue cracks *in situ* induced large, abrupt changes in transient growth rates. The environment influences the nature of the bridging zones, with uncracked-ligament bridges playing a larger role in dry atmospheres, while frictional bridges are predominant in moist air. Evidently, to achieve optimal toughness in bridging ceramics, the window for the requisite grain-boundary strength may be small; whereas weak boundaries are required to induce the necessary intergranular fracture, if too weak, shallower *R*-curves, less strengthening, and poorer fatigue resistance all follow.

I. Introduction

While it has been known for more than 40 years that moisture affects the fracture behavior of alumina,[1–6] there have been few studies seeking to gain a micromechansitic understanding of how moisture separately affects the intrinsic and extrinsic toughening contributions to polycrystalline Al_2O_3.[7] The intrinsic toughness of a material, K_0, refers to the inherent resistance to fracture, while extrinsic toughening refers to mechanisms that act in the crack wake to lower the local driving force experienced at the crack tip, e.g., via grain bridging or phase transformations.[8–12] Based on results in sapphire and silicate glasses, where extrinsic toughening is absent, it is well known that the presence of moisture serves to lower the intrinsic resistance to crack advance at sub-critical velocities.[1,13,14] Specifically, dissociative adsorption of water molecules at stressed M–O bond sites at the crack tip is thought to assist bond rupture while forming surface hydroxyl groups.[14]

For polycrystalline Al_2O_3, which experiences grain bridging, the effect of moisture on the magnitude of extrinsic toughening has not been widely considered. In a fracture mechanics sense, grains that bridge the crack flanks sustain some of the applied load that would otherwise be experienced at the crack tip, thereby effectively toughening the material by lowering the near-tip stress intensity, K_{tip}, relative to the applied stress intensity, K_{app}, giving the relation:

$$K_{tip} = K_{app} - K_{br} \tag{1}$$

where K_{br} is the bridging stress intensity. Grain bridging occurs as a result of intergranular fracture, and accordingly, the boundaries must be sufficiently weak to provide a preferential crack path. It is expected that in the presence of moisture, the intrinsic boundary toughness is lower at low crack velocity. Assuming a pull-out-based model in which the maximum pull-out distance of the grain-bridging zone is invariant, such a moisture-induced reduction in crack-tip toughness would increase the steady-state bridging, as $K_{br} \propto 1/K_{tip}$,[7,15,16] but may flatten the early *R*-curve. However, it is conceivable that the intrinsic boundary toughness, K_{gb}, is reduced more than is the grain toughness, K_{sx}, by the presence of moisture, allowing for more high-angle deviations from the mode I crack path, possibly giving a more tortuous path, more bridging, and less transgranular fracture. Indeed, for some alumina-based materials, the fracture surfaces reportedly appear more intergranular and rougher after subcritical extension than for near-critical crack growth, consistent with *moisture reducing the relative toughness* of the boundaries for slower cracking.[17,18] As a consequence, added toughening effects from more tortuous fracture and more extensive bridging could be anticipated to ensue by lowering the boundary toughness in polycrystals. This would agree with behavior in composites, in which it is established that lowering the fiber–matrix toughness or sliding resistance yields more pull-out and greater net toughening.[19–21]

For the case of cyclic fatigue, while moisture effects have never been formally addressed, a similar situation may be expected as both intrinsic and extrinsic toughening mechanisms play pivotal roles in the fatigue of most engineering materials.[12,22] Cyclic fatigue in Al_2O_3 occurs by degradation of grain bridging in the crack wake.[23,24] Specifically, the bridges tend to wear, chip, and fracture, which raises the local stress intensity at the crack tip (by lowering K_{br}) enough to cause crack advance. In alumina, the local mechanism for cracking at the tip is thought to be identical to that for monotonic loading at the appropriate crack velocity, *v*, with crack advance occurring whenever the intrinsic toughness is locally encountered at the crack tip, i.e., where $K_{tip} \geq K_0(v)$. The most important parameter for fatigue of ceramics typically has been thought to be the fatigue threshold, ΔK_{TH}, which represents the stress-intensity range, $\Delta K = K_{max} - K_{min}$, below which cracks do not propagate. Here, K_{max} and K_{min} represent the maximum and minimum stress intensities experienced during the loading cycle, respectively.

P. Becher—contributing editor

Manuscript No. 20078. Received August 31, 2004; approved January 31, 2005.
Work supported by the Director, Office of Science, Office of Basic Energy Science, Division of Materials Sciences and Engineering of the U.S. Department of Energy under Contract No. DE-AC03-76SF00098.
*Member, American Ceramic Society.
**Fellow, American Ceramic Society.
†Current address: Department of Mechanical Engineering, Oregon State University, Corvallis, OR 97331.
‡Author to whom correspondence should be addressed. e-mail: RORitchie@lbl.gov

However, is it now recognized that thresholds may not be straightforward to utilize in design, being much too conservative for very short cracks, whereas long-crack thresholds are unduly optimistic.[25] Thus, moisture is expected to play a complex role in fatigue, whereby its presence should act to lower the intrinsic cracking resistance (i.e., $K_0(v)$) while also affecting the magnitude of bridging through effects on both bridging geometries and possibly on friction and wear coefficients.

Consequently, the present goal is to investigate the roles of moisture in affecting the fracture and cyclic fatigue properties of polycrystalline Al_2O_3, with attention paid to competing or offsetting effects on the active intrinsic and extrinsic toughening mechanisms.

II. Experimental Procedures

(1) Materials

Experiments were conducted on a 99.5% pure alumina (AD995, Coors Technical Ceramics Co., Oak Ridge, TN), having a wide grain size distribution with a roughly 25 μm average.[25] Compact-tension C(T) specimens, with nominal width, W, and thickness, B, of 17 and 3 mm, respectively, were machined from 21×21 mm square, 10 mm thick blocks and lapped to a 1 μm finish on both sides using diamond compounds. Initial notch lengths were typically $a_0 \approx 4.5$–5 mm, while at the end of each, a razor micronotch was emplaced by repeatedly sliding a razorblade over the saw cut notch in the presence of a 1 μm diamond slurry. Such micronotches typically had root radii of $\rho \sim 10$–15 μm and were used to (1) initiate crack extension at the lowest possible driving forces and (2) minimize the effects of the notch on the stress intensity experienced by very short (<60 μm) cracks. Further details on sample characterization and testing procedures are given in Kruzic *et al.*[25]

(2) Testing Environment

Moist air tests were performed in room air at 25°C, with relative humidity that ranged from 20% to 50%. Conversely, to investigate the role of moisture, tests were also conducted in a flowing dried nitrogen gas environment, also at 25°C. Specifically, 99.999% pure N_2 was passed through a commercial purifier (Gatekeeper, Aeronex, San Diego, CA) rated to purify to sub parts per billion (ppb) levels of moisture, and then through the stainless-steel and aluminum testing chamber. To minimize moisture being picked up from the walls of the metal tubing and testing chamber components, baking-out procedures were used. First the tubing and chamber were heated to ~ 150°C, with dried N_2 flowing throughout the heating process, at which point the chamber was evacuated to ~ 1 Pa using a roughing pump and backfilled with dried N_2 three times. After this rinsing process, the chamber was cooled back to room temperature and allowed to sit overnight with dried N_2 flowing through it prior to each test. In order to estimate the flowing-gas moisture content, an experiment was run by flowing the 99.999% pure N_2 through the purifier, then through a flexible stainless-steel tube that *did not* undergo the bake-out procedure, and finally into a trace moisture analyzer (Tracer, Meeco Inc., Warrington, PA) with 1 ppb sensitivity. This experiment indicated moisture levels below 50 ppb after flowing overnight through this "dirty" tube. It is thus reasoned that the typical gas purity during the cracking experiments was better than 50 ppb of moisture. Finally, some additional dry environment experiments were conducted *in situ* in a field-emission scanning electron microscope (FESEM) under high vacuum ($<5 \times 10^{-4}$ Pa).

(3) Fracture and Fatigue Testing

To determine the R-curve, i.e., fracture resistance, K_r, as a function of crack extension, Δa, in both room air and dried N_2 environments, notched samples were first pre-cracked by cycling (as described below) while occasionally raising K_{max} until the onset of cracking, as revealed by an increase in compliance (i.e., slope of the back-face strain versus load curve). Fatigue pre-cracked samples were re-loaded in displacement control using servo-hydraulic test machines while episodically unloading by ~ 10–20% of the peak load to ascertain the crack lengths.[26] Crack lengths were monitored during the occasional partial unloading based on strain gauges mounted on the back face of the specimen along with standard C(T) compliance calibrations.[27] Due to crack bridging, errors were invariably incurred in the compliance-crack length measurements; accordingly, renormalization to the actual crack length, a, was periodically achieved using optical microscopy on unloaded samples with discrepancies corrected by assuming that the error accumulated linearly with crack extension. Fatigue pre-cracks were grown only to $\Delta a_f = 20$–200 μm prior to measuring R-curves to minimize the initial bridging, where Δa_f is the length of the fatigue-crack extension from the machined notch, i.e., $\Delta a_f = a - a_0$. Additional R-curve experiments were performed in displacement control in an FESEM using a screw-driven loading stage where crack lengths were directly measured from the SEM image of a polished side of the sample.

Cyclic fatigue-crack growth rates were measured in room air and dried N_2 environments in general accordance with ASTM standard E647.[28] Tests were conducted at a frequency of 25 Hz (sine wave) using computer-controlled servo-hydraulic testing machines at a positive, constant load ratio (ratio of minimum to maximum loads) of $R = 0.1$. Crack lengths were continuously monitored by compliance methods, described above. Fatigue-crack growth rate versus applied stress-intensity range (i.e., da/dN–ΔK) relations were assessed using decreasing loading schemes (i.e., under decreasing ΔK conditions); ΔK_{TH} fatigue thresholds were operationally defined as the applied ΔK corresponding to growth rates below $\sim 10^{-10}$ m/cycle. Tests were conducted utilizing continuous automated load shedding that limited the ΔK gradient ($[d\Delta K/da]/\Delta K$) to roughly -0.08 mm^{-1}. Ideally, this rate of change in loads would be sufficiently slow to allow the crack bridging levels to adjust to the current level of ΔK, thereby yielding the steady-state growth curve; however, due to the large, several millimeter, cyclic bridging zones formed by this Al_2O_3 in moist air, such steady-state conditions were only achieved (in moist air) below growth rates of $\sim 10^{-8}$ m/cycle.[25] In dried nitrogen, where a less extensive bridging zone may be expected, such constraints would not be as severe; thus, fair comparisons of steady-state fatigue-crack growth rates may be made for $da/dN \leq 10^{-8}$ m/cycle.

(4) Crack Profiles and Fractography

Qualitative observations of crack paths and fracture surfaces were made using the FESEM. Additionally, to assess the magnitude of bridging, the crack-opening displacements, $u(x)$, were measured quantitatively on samples loaded *in situ* in the FESEM, where x is the position along the crack wake with origin at the load line. Such results can be compared with the crack opening for a bridge-free crack at the same applied driving force, u_{app}, computed using:[29]

$$u_{app}(x) = \frac{1}{E'} \int_x^a K_{app}(a') h(a', x)\, da' \tag{2}$$

where E' is the modulus (E in plane stress, $E/(1-\nu^2)$ in plane strain, assumed here, and ν is Poisson's ratio), h is a geometry-dependent weight function and $K_{app}(a)$ refers to the K-crack length relation for that same geometry. Furthermore, the crack-opening displacement data were used to directly deduce estimates for the intrinsic toughness, K_0, using two methods.[30,31] Specifically, the measured displacements were first related to the near-tip stress intensity via:[30]

$$u(x) = \frac{\bar{K}_{tip}(x)}{E'} \int_x^a h(x, a')\, da' \tag{3}$$

This can readily be done for each $u(x)$ value giving an associated set of apparent values of $\bar{K}_{tip}(x)$; these are then extrapolated to give the pertinent value at the tip. For a crack loaded just at criticality:

$$\lim_{x\to a} \bar{K}_{tip}(x) = K_0 \tag{4}$$

Alternatively, additional data than just those giving the limit for $x \to a$ were more rigorously considered using a two-term solution for the shape of a bridged crack:[31]

$$u(x) = \frac{K_0}{E'}\int_x^a h(x,a')\,da' + \frac{A_1}{E'}\int_x^a (a-a')h(x,a')\,da' \tag{5}$$

where the unknowns K_0 and A_1 may be determined using a least-squares fit to the experimental $u(x)$ data. In both cases, h for the C(T) specimen was used, viz:[32]

$$h = \sqrt{\frac{2}{\pi a}}\frac{1}{\sqrt{1-x/a}} \times \left[1 + \sum_{(\nu,\mu)} \frac{A_{\nu\mu}(a/W)^{\mu}}{(1-a/W)^{3/2}}(1-x/a)^{\nu+1}\right] \tag{6}$$

where the coefficients $A_{\nu\mu}$ are given in Fett and Munz.[32]

III. Results

(1) R-Curve Results

Figure 1 compares *R*-curve results from moist air and dry environments at ambient temperature, based on three specimens tested in air, four in dried N_2, and two in vacuum (*in situ* FESEM). For the dry situations, only one specimen (in N_2) yielded data after the crack extended beyond $\Delta a = 1$ mm due to difficulties in extending cracks beyond this point without catastrophic failure. The *R*-curve initially rises much more steeply in the dry environments (see Fig. 1 inset). Once cracks have extended for 2–3 mm, the *R*-curve behavior in air and dried N_2 becomes almost indistinguishable, although it is cautioned that the samples used were not large enough to allow accurate determination of these *R*-curves for very long cracks, i.e., at steady-state levels. However, the greater stability of samples tested in air indicates that the *R*-curves do actually cross, implying that the steady-state toughness is greater for moist conditions.

(2) Fatigue Results

Fatigue-crack growth data for long cracks ($\Delta a_f > 2$ mm), in the form of da/dN–ΔK plots, are shown in Fig. 2 for samples tested in moist air and dry N_2. While there is some scatter within each data set, which is typical for ceramics due to the stochastic nature of bridging, the steady-state growth rates are similar in each environment.

Although these experiments in a fixed environment do not indicate any clear effect of moisture on the steady-state fatigue behavior, the situation differs with individual specimens when the environment is suddenly changed during crack propagation at a constant ΔK. Figure 3(a) shows crack length versus cycles data for a specimen where a long fatigue crack, initially growing in dried N_2, was suddenly exposed to moist laboratory air by opening the testing chamber; this exposure resulted in an abrupt three orders of magnitude increase in (transient) growth rate, from $<10^{-10}$ to 2×10^{-7} m/cycle. Since at the instant of the change, the bridging contribution in the crack wake would be expected to remain essentially unchanged, this sudden increase in fatigue-crack growth rate is attributed to a decrease in K_0 upon exposure to moist air. The reverse experiment was also conducted (Fig. 3(b)) whereby a crack growing in moist air was switched into dried N_2, although not instantaneously as cycling was stopped to purge and bake out the chamber. Here, a greater than three orders of magnitude decrease in transient crack-growth rate ensued, from 2×10^{-7} to $<10^{-10}$ m/cycle, which can be attributed to an increase in K_0 in the dry environment. In actuality, for the latter experiment, the crack essentially arrested; however, growth at rates below $\sim10^{-11}$ m/cycle cannot be ruled out due to the resolution of the crack-monitoring method.

Another alteration in the fatigue behavior with change in environment was the significant difference between the compliance curves (Fig. 4). Compliance curves for samples tested in moist air exhibit considerable hysteresis, typical of those for bridging ceramics with frictional crack-face interactions,[33,34] while the curves for tests in dried N_2 showed no detectable hysteresis, and were linear except at the lowest loads, where premature crack

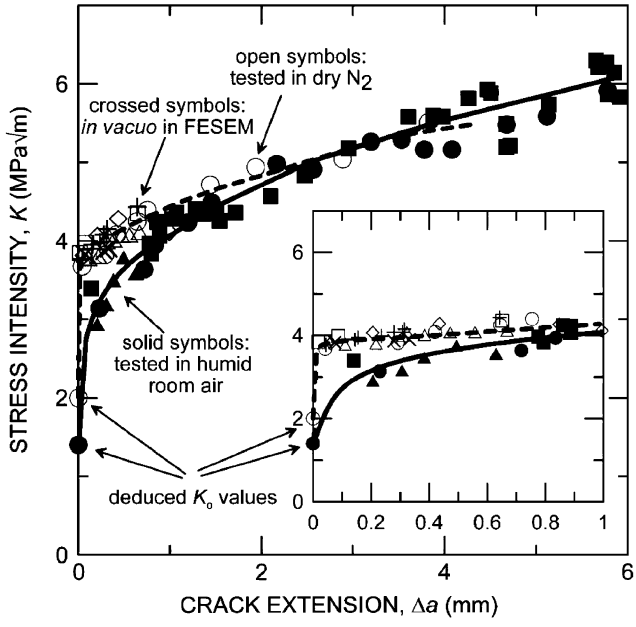

Fig. 1. *R*-curves for Al_2O_3 C(T) samples tested in dry N_2, vacuum in an FESEM, and moist air. Inset magnifies behavior at initial crack extensions. Note the much more steeply rising *R*-curves in inert atmospheres.

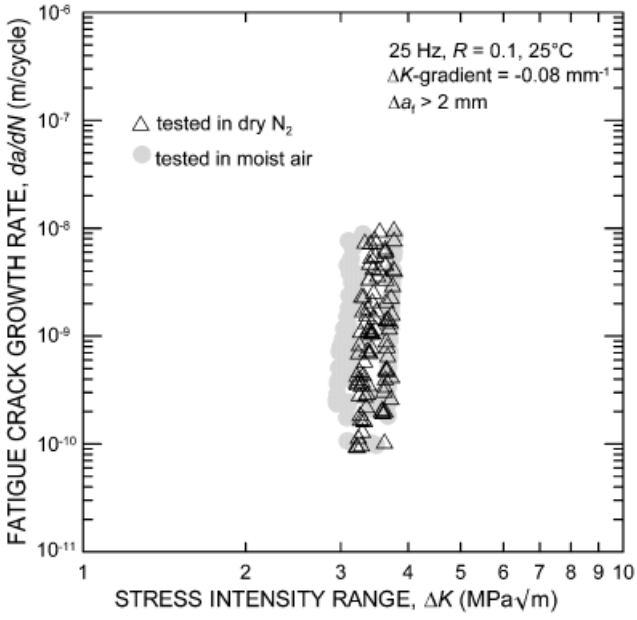

Fig. 2. Comparison of steady-state fatigue-crack growth rates for long cracks (>2 mm) in Al_2O_3 tested in moist air and dry N_2. Growth rates are essentially identical in both environments.

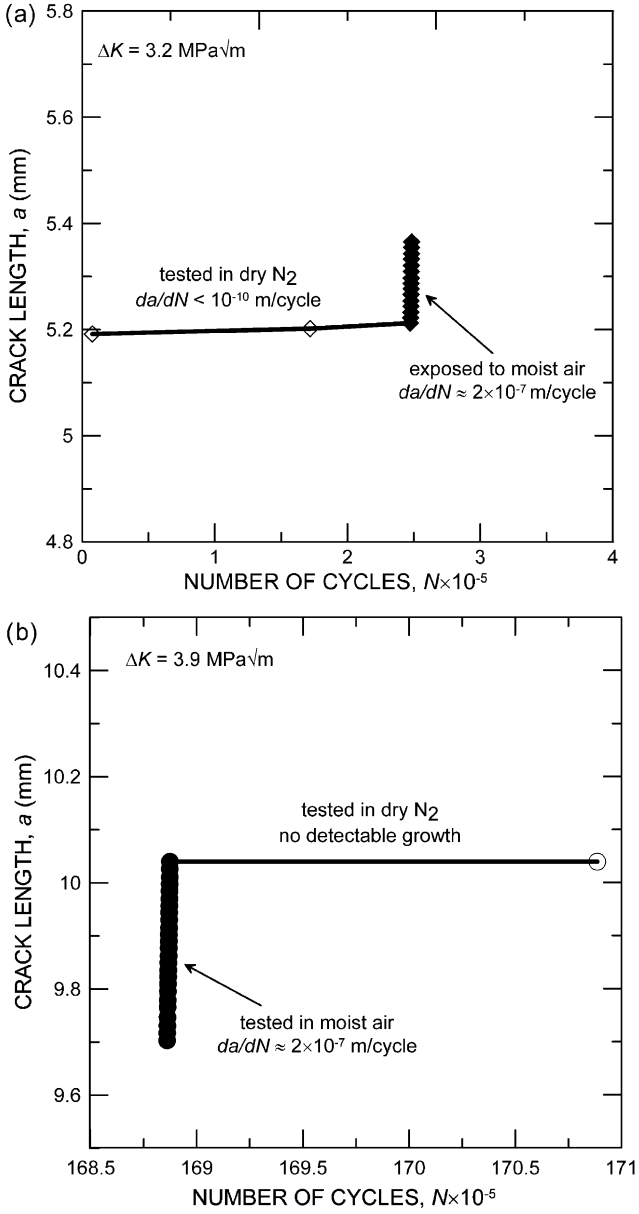

Fig. 3. Results show more than three orders of magnitude immediate change in fatigue-crack growth rates at a constant ΔK upon changing the environment from (a) dry N_2 to moist air and (b) moist air to dry N_2.

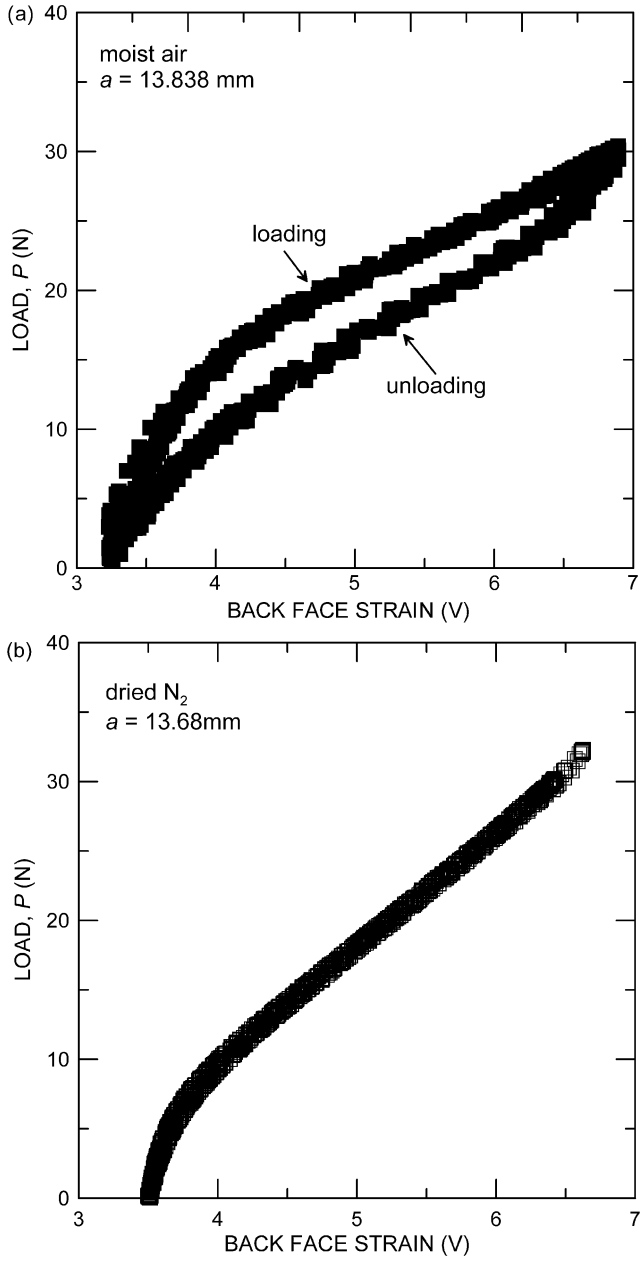

Fig. 4. Comparison of compliance curves for fatigue cracks grown in moist air and dry N_2 shows an absence of hysteresis for the dry case. This implies that there is much less frictional bridging in inert atmospheres. Strain units are arbitrary voltages. Crack lengths are computed from the unloading curve in the long linear region.

closure caused notable nonlinearity. Such results imply that significant differences exist in the nature of the bridging in samples tested in moist versus dry atmospheres.

Such differences in the bridging could not be detected by fractography; FESEM examination revealed no obvious differences in fracture morphology from any stage in the *R*-curve or from fatigue (e.g., Fig. 5). To confirm the similarity in appearance of the fracture surfaces, one sample was cycled while alternating the environment between moist air and dried N_2 after every few millimeters of crack growth. The purpose was to create detectable bands on the crack surface if the morphology changed with the environment; however, the fatigue fracture surface appeared uniform in the FESEM at all magnifications.

In contrast to the fatigue-crack growth results in Fig. 2 for long, steady-state cracks ($\Delta a_f > 2$ mm), the behavior of short cracks ($\Delta a_f \sim 20$–60 μm) grown from razor micronotches reveals large differences between crack growth in moist air and dried N_2 environments (Fig. 6). Specifically, in each case, growth would initiate at some ΔK level but rapidly arrest for short cracks; the driving forces needed to grow similar-sized cracks in N_2 were some 60–70% higher than in moist air. As the bridging zone is not fully developed for such short cracks, the role of the intrinsic mechanisms is accentuated, such that a decrease in K_0 in the presence of moisture leads to accelerated growth. In addition, if the development of the bridging zone during extension of short cracks differs in the two environments, as is seen for the *R*-curves (Fig. 1), such effects will be accentuated here as well.

(3) Crack-Opening Profile Results

Figure 7 shows crack-opening profiles (COPs) for fatigue cracks in two samples with nominally the same geometry and crack length, $W = 17.1$ mm, $a = 13.8$ mm, loaded *in situ* to $K = 3.0$ MPa $\cdot$ m$^{1/2}$. During prior fatigue testing, cracks in each had been grown near the long-crack fatigue threshold ($\leq 7 \times 10^{-10}$ m/cycle) for the last 3 mm (i.e., further than the 2 mm bridging-zone length previously seen in moist air[25]). This ensured that the measured openings were for the near-threshold steady-state case, as the nature of the bridging zone is a function of prior loading conditions. For both samples, the crack openings are

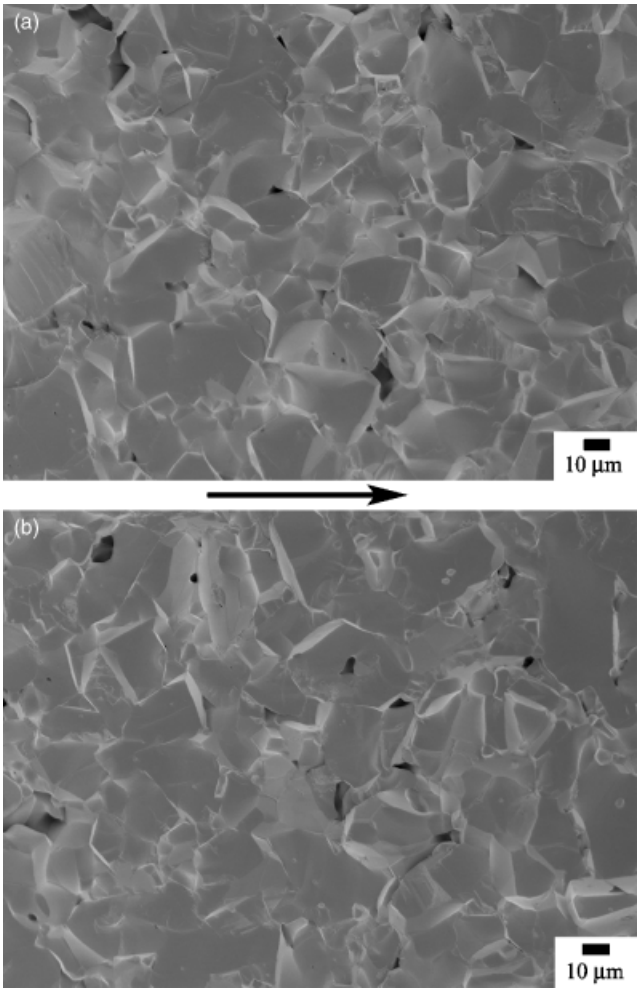

Fig. 5. Scanning electron micrographs of fatigue fracture surfaces for samples tested in (a) moist air and (b) dry N_2. Arrow indicates the general direction of crack growth.

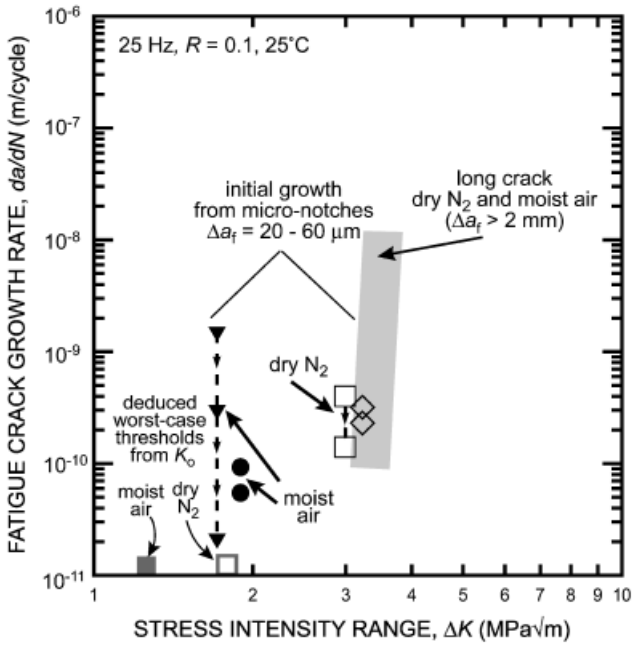

Fig. 6. Comparison of fatigue-crack growth rates from short (20–60 μm) cracks emanating from razor micronotches in moist air and dry N_2; each symbol represents an individual specimen. Although velocities for steady-state cracks (>2 mm) exhibit no apparent environmental effect, a significant effect exists for short cracks. Predicted worst-case fatigue thresholds are based on deduced K_0 values.

smaller than that computed using the weight-function method for a bridge-free crack, Eq. (2), indicating that bridging is active in each case. Also, the near-tip crack opening in dried N_2 is somewhat larger than in the moist air.

Additional crack-opening displacements were measured for one *R*-curve specimen, loaded to induce extension in air using the loading stage, before placing it into the FESEM. The sample was loaded sufficiently to induce moisture-affected crack growth (at $K_{app} \approx 4.0$ MPa $\cdot$ m$^{1/2}$), before some load relaxation occurred owing to further subcritical growth in air while at fixed displacement (yielding a final $K_{app} \approx 4.6$ MPa $\cdot$ m$^{1/2}$). (These COP results are not in Fig. 7 as comparisons are meaningless due to differences in the applied driving force and crack size.)

Based on the crack openings, estimates of K_0 were made using the methods described above (Section II(4)). The COP was measured for the *R*-curve specimen while at the load used to produce extension, but the fatigue samples were re-loaded for COP measurements to only 73% of the load used for crack extension, i.e., the moist and dry samples had each been previously loaded in fatigue to $K_{max} = 4.1 \pm 0.1$ MPa $\cdot$ m$^{1/2}$. Accordingly, the additional 27% (1.1 MPa $\cdot$ m$^{1/2}$) must be added back to K_{app} to get a realistic estimate of K_0. This additional stress intensity must be split between K_{tip} and K_{br}, Eq. (1), which was alternately carried out by assuming that K_{tip} and K_{br} would rise proportionally, or that K_{br} was saturated and the remaining loading would raise only K_{tip} (an upper-bound estimate to K_0); the average was taken leaving a range of uncertainty for each estimate. Results for K_0 successively based on the single-term method, Eqs. (3)–(4), and the two-term method, Eq. (5), are given in Table I, and both indicate that removing environmental moisture yields an increase in the intrinsic toughness, K_0. In some cases, the single-term method gave a slightly lower (0.2 MPa $\cdot$ m$^{1/2}$) average value than did the two-term method; the two-term method is considered to be more accurate and those results are used for further discussion. The two-term analysis was based on fitting the first 1.5 mm of COP data (3/4 of the $u(x)$ values shown in Fig. 7); this gave values of K_0 and A_1 that were relatively insensitive to the number of points used. Attempts to fit more points gave statistically less reliable parameters, suggesting that another term is then needed from the expansion[32] used to account for the bridging effect on the COP. The extrapolations using the one-term results were derived from a similar number of these data points, but resultant values were not so different from the last few values from just near the tip.

Using these methods, the average K_0 for samples tested in humid air was 1.4 MPa $\cdot$ m$^{1/2}$, while for dried N_2, K_0 was 2.0 MPa $\cdot$ m$^{1/2}$, some 0.6 MPa $\cdot$ m$^{1/2}$ higher. These deduced (average) K_0 values are plotted as the initiation points on the *R*-curves in

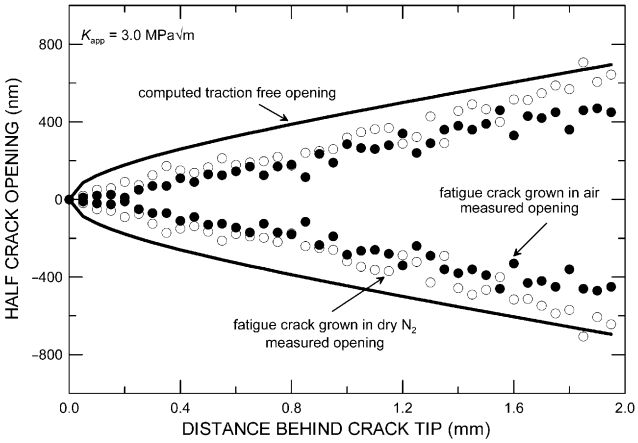

Fig. 7. Measured crack-opening profiles at $K_{app} = 3$ MPa $\cdot$ m$^{1/2}$ for fatigue cracks grown in dry N_2 and moist air are compared with the computed opening for a linear-elastic traction-free crack.

Table I. Estimates of the Intrinsic Toughness, K_0

Environment	One term, Eqs. (3)–(4) ($MPa \cdot m^{1/2}$)	Two term, Eq. (5) ($MPa \cdot m^{1/2}$)
Moist air (*R*-curve)	1.4	1.4
Moist air (fatigue)	$1.2 \pm 0.3^{\dagger}$	$1.4 \pm 0.3^{\dagger}$
Dried N_2 (fatigue)	$1.8 \pm 0.3^{\dagger}$	$2.0 \pm 0.3^{\dagger}$

[†]Ranges reflect the different methods used to add the additional stress intensity to achieve criticality—see text for details.

Fig. 1 and used as K_{max} to plot the worst-case fatigue thresholds, ΔK_{TH}, for the absence of bridging in Fig. 6, i.e., as $\Delta K_{TH} = K_0(1-R)$ to reflect the load ratio of $R = 0.1$ used here.

IV. Discussion

Crack-propagation resistance derives from the sum of intrinsic mechanisms operating at and ahead of the crack tip and extrinsic shielding mechanisms from the wake, although the total can reflect a degree of mutual competition between these classes.[12,22] Changing the crack size, microstructure, and environment can markedly influence crack-growth behavior through their influence on these mechanisms, which, however, may differ on each mechanism. A better understanding of these effects can be obtained by (i) characterizing and quantifying such crack bridging, (ii) suddenly changing the environment to immediately change only K_0, and (iii) deducing K_0. Although the role of moisture in influencing steady-state fatigue-crack growth in this Al_2O_3 appears to be minimal (Fig. 2), further investigation reveals that the specific intrinsic bond-rupture mechanisms and extrinsic (bridging) mechanisms are both affected, but in opposite ways by the presence of moisture, with the detrimental effect on K_0 being balanced by its positive effect in promoting crack bridging. However, the strong net effects of atmosphere on short cracks are key findings with implications regarding strength and lifetime that do not follow simply from the compensating behavior for steady-state cracks.

The extrinsic mechanisms and their influence on reliability will be examined after assessing the intrinsic toughness. First, we note that although it is not usually considered as such, the *R*-curve in bridging ceramics should necessarily initiate at a level appropriate for cracking a grain-boundary facet, K_{gb}, and so below that to crack a grain (i.e., a single crystal), K_{sx}, and then eventually rise as bridging develops until possibly attaining a steady-state value. However, this situation is clouded by two factors, namely: (i) for a very *small* crack having all areal dimensions of the order of the grain size, the effects of local residual stresses, e.g., from thermal expansion mismatch, may influence the effective toughness, even lowering it below that for the boundary facet for a critical flaw;[7,15,16] or (ii) for a very *short* crack, which, in the hypothetical limit is a ribbon of through-thickness crack but with a being less than a grain facet long, the residual stress effects tend to cancel, but the inevitable kinks and twists raise the initiation toughness above the average for the actual boundary facets.[§] Regardless, *the early part of the R-curve and the short-crack fatigue curves are most important for reliability and strength,* although they are rarely measured accurately, if at all. Steep initial slopes are highly desirable for *R*-curves because allowable flaws in ceramics are necessarily small due to the low toughness; hence, materials that achieve their peak toughness at small crack lengths are preferable.

(1) Intrinsic Effects: Estimation of K_0

Table I gives estimates of the intrinsic toughness K_0 for this alumina tested in both moist and dry environments. The value of K_0 may be elevated relative to K_{gb} somewhat due to the three-dimensional nature of the present cracks from local kinking through the sample thickness. In this regard, an estimate of $K_0 \approx 2.0 \pm 0.3$ $MPa \cdot m^{1/2}$ for inert environments appears quite reasonable, as this is lower than the critical toughness of sapphire ($\sim$2.2–2.6 $MPa \cdot m^{1/2}$ for all planes but those near (0001), which do not cleave,[3,35–37]), and is above the toughness measured for typical oxide glasses (i.e., < 1 $MPa \cdot m^{1/2}$).[38–41] The estimate of $K_0 \approx 1.4 \pm 0.2$ $MPa \cdot m^{1/2}$ for moist air also appears reasonable, being $\sim 0.7 \pm 0.2$ of the inert value. This shift to lower K_0 with increasing moisture is consistent with crack-growth behavior in sapphire[1,3] and various silicate glasses,[13,42,43] although apparent threshold values in moisture are typically lower fractions of the fast fracture (or dry) levels of K_c, being 0.5,[1,3] 0.5–0.6,[2,6] and $\leq$0.3,[13,42,43] for one plane of sapphire, polycrystalline alumina, and silicate glasses, respectively.

Assuming the deduced K_0 values, being for short ribbon cracks, somewhat exceed the actual toughness values for boundary facets, then it implies that the true K_{gb} values are sufficiently less than the respective values for sapphire, K_{sx}, for both dry and moist conditions to allow extensive boundary fracture, in keeping with the predominantly intergranular fracture path found here in each atmosphere (Fig. 5). Based on a 2-D model,[44] if the ratio $K_{gb}/K_{sx} < 0.5$, then kinking could occur readily to allow a crack to deflect onto any intersected grain boundary, and so the fracture should be entirely intergranular, which is not quite seen here, possibly owing to the simplicity of a 2-D consideration or to K_{gb}/K_{sx} not being quite so low.

It should be noted that the estimate of K_0 based on the fatigue crack tested in moist air in Fig. 7 is somewhat lower than that of a previous study on the same alumina, which gave $K_0 \approx 1.6 \pm 0.15$ $MPa \cdot m^{1/2}$ by first deducing a bridging stress distribution (based on the same COP data plus measured compliance changes from cutting out the crack wake), computing K_{br} from it, and then applying Eq. (1).[25] Identical methods were attempted here for a sample tested in dry N_2, but it was too fragile to withstand the multicutting procedures to progressively machine away the crack wake. In order to use the same procedures for both the present moist and dry tests, analysis methods were chosen based on direct fits to the experimental COPs using Eqs. (3)–(4) or (5). Another advantage of the present methods is that any assumptions made in deducing a bridging stress distribution are avoided.

It is insightful to compare these K_0 values with other results. One set of alumina samples, having a range of grain sizes and likely being somewhat purer (i.e., sintered without additives), was examined extensively[45–47] giving K_0 values spanning 1.8–2.6 and averaging 2.3 $MPa \cdot m^{1/2}$.[45,47] These were obtained from COPs resulting from monotonic loading by fitting only the near-tip region to the traction-free, parabolic elastic crack-opening profile from Irwin (assuming, implausibly, the fitted region to be ahead of all the active bridging). A re-analysis of some of these gave $K_0 \sim 2.2$–2.5 $MPa \cdot m^{1/2}$ by using the same one-term method as here, Eqs. (3)–(4);[30] this corrects the COP in the finite length increment that being well outside the *K*-field depends on sample geometry, but does not account for any bridging effects. Another study of an Al_2O_3 containing large-scale Al reinforcements found K_0 values of 2.4–2.5 $MPa \cdot m^{1/2}$ by fitting COPs to the parabolic (Irwin) relation.[48,49] In principle, the two-term method from Eq. (5) should be preferable as it explicitly attempts to describe the COP in finite crack regions that are beyond the *K*-field and also experience bridging forces; these adjustments are needed because significant bridging develops on the same length scale as accurate COP measurements can be made (compare Figs. 1 and 7). Indeed, fitting the crack profile to a parabolic relation was unsuitable in the present study as the initial COP data in Fig. 7 are more nearly linear.

The results of those other studies based on the COP of undoped samples first loaded to criticality in ambient air gave higher values of K_0 than were found herein for moist or dry samples, even when using the same analysis method, Eqs. (3)–(4). This is not unreasonable considering that Auger electron

[§]The terminology used here is that *short* cracks are small only with respect to length, whereas *small* cracks are small with respect to width and length.

spectroscopy studies in a companion investigation revealed Ca along the grain boundaries in this 99.5% Al_2O_3 (versus the silicates being found in the glassy pockets);[50] Ca may lower K_{gb} and K_0, which may then lead to more bridging, as was also proposed by others.[51] As the efficacy of these various methods to deduce K_0 is just being explored, there is yet inadequate experience to confidently assess the systematic or random errors in K_0 values deduced from a COP either directly or after computing K_{br}. Nonetheless, the resulting trends are reasonable and encourage pursuing such studies. However, one may note that the purer samples, for which K_0 was found to average 2.3–2.5 $MPa \cdot m^{1/2}$, usually exhibited intergranular fracture and bridging;[45–47] this suggests that these values must somewhat exceed the average K_{gb} in order for it to be sufficiently less than K_{sx} for such fracture, although residual stresses may also influence the crack paths. Finally, for comparison, similar values of $K_{tip} = 1$–2.5 $MPa \cdot m^{1/2}$, again being $\leq K_{sx}$, were also found for an alumina of uncertain purity sometimes containing various SiC reinforcements by assessing the near-tip stress field using the Raman shift measured with optical microscopy.[52]

(2) Extrinsic Effects: Bridging-Zone Development

The rising *R*-curve behavior in Fig. 1 and the crack-opening results in Fig. 7 demonstrate that active bridging ensues during fracture and fatigue in both humid and dry environments. Under both loading types, however, a useful bridging contribution develops far more quickly in dry atmospheres. Indeed, in the dry environments, the *R*-curves rise more steeply (Fig. 1) and short fatigue cracks (20–60 μm) are more resistant to growth (Fig. 6) by a magnitude exceeding the 0.6 $MPa \cdot m^{1/2}$ deduced difference in K_0. Similarly, in Si_3N_4, increases in grain-boundary strength derived using different additives have been found to yield initially steeper *R*-curves.[53]

Since weaker boundaries should allow for more crack deflections, and accordingly more frictional bridging development, the differences in behavior may instead be related to some morphological differences, perhaps in the development of uncracked-ligament, or elastic, bridges. Both uncracked-ligament and frictional bridging are readily observed in the fracture and fatigue of polycrystalline aluminas, with the former developing and exhausting closer to the crack tip, and the latter extending further into the crack wake.[24,25,54,55] Uncracked-ligament bridges are usually seen as regions of intact material between non-coplanar crack segments, often several grain diameters in size, in the wake of a crack tip that forms as a result of either non-uniform advance of the crack front (leading to segments subsequently sweeping under and over one another), or perhaps nucleation of microcracking ahead of the main crack tip. Measurements using X-ray fluorescence and Raman spectroscopic techniques on an alumina and a Si_3N_4 have shown a large abrupt drop in bridging stress beyond the regions containing uncracked-ligament bridges, suggesting that these bridges sustain markedly higher stresses than do frictional bridges further behind in the trailing crack wake.[55,56] Similarly, bridging stress distributions computed iteratively to match the COPs measured by interferometry in a similar alumina exhibited a very rapid drop after a small crack opening and a long persistent tail.[57]

While qualitative observations in the FESEM showed that uncracked-ligament and frictional bridges occur in these alumina samples tested in both environments, such observations have not provided the quantitative evidence needed to deduce a difference in the nature of the bridging. Pertinent evidence emerges, however, by comparing the compliance curves for tests in each environment (Fig. 4). Specifically, the lack of hysteresis for the fatigue tests in dry N_2 implies that active frictional bridging is limited, although the COP (Fig. 7) shows that bridging is significant. Since uncracked-ligament bridging should not cause as much hysteresis in the measured compliance, one may conclude that uncracked-ligament bridging provides a higher proportion of the toughening in the absence of humidity. Moreover, because fractured boundaries would be expected to exhibit higher frictional coefficients in the absence of moisture,[58] hysteresis in the dry environment should be more, not less, pronounced if frictional bridges were predominant for both the humid and dry cases.

Although uncracked-ligament bridges are known to operate nearer to the crack tip than do frictional ones,[24,25,54,55] there is no accepted prototypical model that would rationalize that such bridges should be so strong or cause such a rapid rise in resistance to further crack extension. It is important that the steepest rise in these *R*-curves occurs over a dimension of about the average grain size in dry atmospheres, as opposed to a length of five times that in the moist situation (Fig. 1, inset). Thus, the uncracked-ligament mechanism seems to be initially more potent than might be expected from the cantilevered, uncracked sections that are often observed in the crack wake after two crack segments have swept past one another, as is also discussed elsewhere.[59] However, this configuration, observed on polished sections, develops long after the rise in load-bearing capacity found here. Hence, the key event that distinguishes the two types of bridging must occur at an earlier stage, perhaps as a crack front first bifurcates with separate parts kinking up and/or down to follow local boundary paths. At that stage, an intervening region still connects the two regions. If K_{gb} is low enough, this link can tear, primarily in mode III loading; further extension could then entail extensive cracking around single grains that would lead directly to frictional bridging. Perhaps, instead if the K_{gb} were just too high, such connecting regions would not immediately crack, instead causing the two bifurcated crack segments to extend independently, becoming non-coplanar, and later, sweeping past each other leaving the well-observed cantilevered element. Some analyses of the toughness arising from rough intergranular fracture or from a cleavage fracture encountering a grain boundary posited that the segments of mode III extension contribute a major portion of the fracture resistance.[60–62] Thus, if such mode III failure cannot occur readily, it could instead trigger a different crack extension sequence needing a rapid rise in load to overcome the closure force from the still intact, connecting link. However, once cantilevered segments begin to form and break in a steady-state process, further load increases are unnecessary in contrast to those expected for frictional pull-out, which develops more slowly, thereby gaining bridging leverage far behind the crack tip.

An alternative hypothesis would be that elastic bridges form simply by nucleation of microcrack segments ahead of the main crack. Such new cracks would likely be off the plane of the main crack if they form at regions of highest principal stress;[63] hence, they could, in principle, extend for some distance on different planes as is often observed for actual elastic ligaments. Such bridges could be stiff and non-hysteretic, but such multiple nucleation events are hard to justify in brittle ceramics in the absence of a spatial distribution of many small flaws, high internal stresses, or some other factor that would effectively yield an exceptionally wide distribution in boundary strengths.[63]

Finally, it must be acknowledged that although the present data, e.g., on transient cracking (Fig. 3), indicate that K_0 is lower in the moist atmosphere, it is ambiguous from those data and additional analysis (Table I) whether K_{gb} is reduced more than is K_{sx}, as would be required to make intergranular fracture more prevalent and alter the bridging mechanism. We conjecture that this is the case, in part based on observations elsewhere that slow crack growth, wherein moisture has the greatest influence, often leads to observably more intergranular fracture than occurs as cracks accelerate but still remain sub-sonic (without having developed the hackle typical of overdriven, rapid fracture).[17,18]

(3) Crack Size Effects and Reliability

The present fracture and fatigue results imply that the relative effects of moisture on the intrinsic and extrinsic toughening are

not constant over all crack sizes. While K_0 is expected to be insensitive to crack size, the moisture effects on K_{br} are not. For cracks $\sim$2 mm long, under both steady-state fatigue (Fig. 2) and quasi-static fracture conditions (Fig. 1), the presence of moisture appears to lower K_0 and raise K_{br} by similar magnitudes leading to small net effects. For very short crack lengths, however, tests in moist air exhibit lower K_0 and K_{br} relative to the dry cases for both fracture (Fig. 1) and fatigue (Fig 6). With the development of a long crack wake, in contrast, the moist air samples experience more crack deflections and thus generate larger amounts of frictional bridging, causing the values of K_{br} and of total toughness to eventually exceed those for dry environments. Compensated behavior is not unlike what has been found for a Si_3N_4 in one study,[64] while another has shown a marked effect of moisture on steady-state fatigue-crack growth behavior,[65] suggesting that effects on K_0 and K_{br} may offset to different degrees depending on the exact material composition, microstructure, crack size, and environment.

By virtue of having deduced useful estimates of K_0 and actually having measured the resistance after as little as $\sim$20 μm of extension for cracks emanating from micro-notches (after which no notch-based correction for K_{app} is needed), it has been possible to construct reasonable estimates of nearly the entire *R*-curve for both wet and dry atmospheres, Fig. 1. These curves, for short (not small) cracks, both initiate at K_0 values ≤ 2 MPa $\cdot$ m$^{1/2}$. These low initiation levels, which are necessary to account for the intergranular facture, are much less than for most reported *R*-curves. In a few instances, especially with fine grain sizes for which K_{br} is small, directly measured *R*-curves appear to initiate at 2.5–3 MPa $\cdot$ m$^{1/2}$,[34,66,67] but all too often, owing to difficulties in assessing short cracks, the first data for *R*-curves appear at even higher levels, which are often beyond interest for controlling strength.

The present results illustrate two sets of behavior: one is the same for either of two dry environments and likely approximates the inert limit, while another is for material in high, but not saturated, humidity at low, but finite, velocities and approaches another limit.[¶] However, complete velocity- and humidity-dependent spectra of behavior must exist under transient and steady-state conditions for monotonic, sustained static, and cyclic loading that remain to be characterized and modeled. An ambitious model from Lathabai and Lawn,[7] Chantikul *et al.*[15] and Bennison and Lawn[16] attempts to do so for monotonic loading, and does illustrate known trends in effects of velocity, residual stresses, and grain size for both short and small cracks. However, this model is too simple in that the bridging pull-out length does not vary with K_0, as it should based on models for fiber/whisker reinforcement,[19–21] and that such shear-lag models poorly approximate pull-out behavior, as indicated from numerical computations, especially for the misaligned grains that actually provide most bridging.[68,69] More critically, the present results reveal an unanticipated complexity—the bridging mechanism itself changes with atmosphere.

The beneficial effects of steeper *R*-curves are illustrated in Fig. 8, which depicts the predicted strength as a function of initial flaw size based on the two *R*-curves in Fig. 1. The strength, σ, was calculated using:

$$\sigma = K_r/\sqrt{\pi a} \tag{7a}$$

$$dK_{app}/da = dK_r/da \tag{7b}$$

In Fig. 8, the initial flaw size, a_i, refers to the full length of a surface flaw, or half-length of a subsurface flaw; this is a conservative strength estimate as the initial flaw is taken to be free of bridging, and criticality only occurs after sufficient extension to satisfy the condition in Eq. (7b). A pronounced difference in predicted strength occurs over the range of expected flaw sizes, due to the greater steepness of the *R*-curve in dry environments,

[¶]Strictly, K_0 is for a near-threshold velocity, and the moist *R*-curve is for a higher velocity, but the differences are thought to be small for present purposes, as are possible velocity effects for the inert limit.

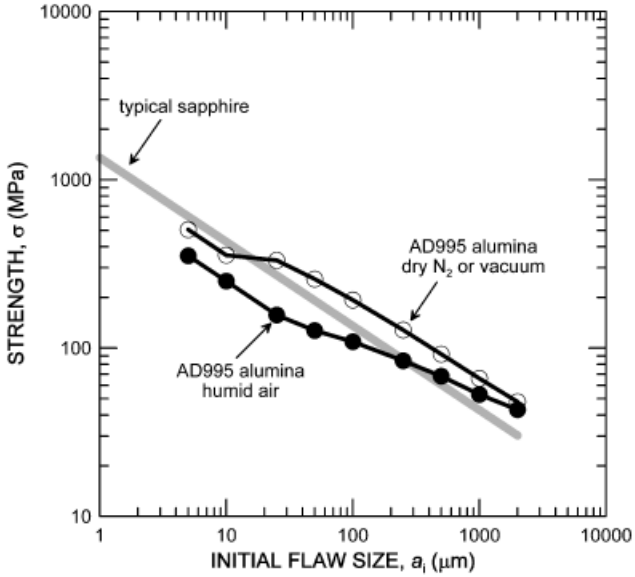

Fig. 8. Plot of predicted strength versus initial flaw size constructed using *R*-curve data in Fig. 1. Note the large improvement in strength at relevant crack sizes (tens of micrometers) expected in dry environments where the grain-boundary strength is higher. The curve for sapphire, being based on the critical toughness, relates better to an inert situation.

while there is negligible difference at sizes of order 2 mm where the benefits of bridging are experienced for both; if flaws were smaller though, the bridging would be of no benefit and the controlling toughness would decrease toward K_0. for each atmosphere. Thus, it is concluded for this alumina that stronger boundaries associated with dry environments are beneficial at the most relevant crack sizes ($\sim$tens of micrometers); moreover, their presence does not appear to cause any degradation in mechanical performance at longer, less relevant, crack sizes until after the *R*-curves have clearly crossed ($\Delta a > 2$ mm).

Such predictions nominally agree with the well-documented effect of humidity in lowering the strength of AD995 and other alumina ceramics.[2,7,70–73] Typically, the observed, associated dependencies on crack velocity and temperature have been implicitly attributed just to effects on $K_0(v)$.[2,71,72] Based on measured differences in K_0 (Table I) or even from *v*–*K* curves in single crystals,[1,3] direct scaling would readily account for a factor of two or less difference in extremes of velocity-dependent strength, which is less than derives with the associated effects of the *R*-curves at some flaw sizes, Fig. 8. Unfortunately, reported strength data do not span a sufficient range of velocity to permit a clear distinction among causes.[2,7,71,72] However, in a study relating crack-growth kinetics and the velocity dependence of uni- and bi-axial strengths, it was found that for a coarse-grained glass ceramic, the differing effects of microstructure precluded a correlation based solely on changes in K_0, as does pertain for glass.[74] We also note that the strengths in Fig. 8 seem low versus those reported in Cho *et al.*[71,72] for similar material, but that if penny-shaped flaws are assumed, which would shift the curves up by 1.57 times, then the two prediction sets would bound the actual observed results.

The effects discussed here should also contribute to the influence of temperature on strength and toughness, although this is more complex as thermally-activated bond rupture[18] and desorption of water both influence K_0, and the shift of thermal expansion mismatch stresses may change tendencies for crack bifurcation. A recent study has examined the effect of elevated temperature on the detailed bridging contribution for a polycrystalline alumina;[57] the long crack bridging and total toughness both decreased with heating, but it is difficult to assess causes or the effect on K_0.

Finally, we reiterate that the short fatigue cracks virtually arrested very rapidly after growth initiated. In either

atmosphere, both minimum detectable crack growth and rapid arrest occur at driving forces well above the deduced minimum needed to cause extension of an unbridged crack, i.e., at $K_{max} = K_0$. The arrest is attributed to the rapid development of bridging, and, as with the strength in monotonic loading (Fig. 8), the benefit of a dry atmosphere well exceeds that from the effect deduced for K_0. As crack arrest occurs after <60 μm of crack extension, arrested cracks can still be small enough that a sample with natural flaws could have significant retained strength under monotonic loading, as can be found from Fig. 8, especially for the inert case. Quite clearly, the use of the shortest crack growth threshold, the minimum driving force for any crack extension, denoted in Fig. 6, is far too conservative to serve as a useful design criterion for bridging ceramics if the *R*-curve develops quickly enough to benefit strength. However, the use of the long crack fatigue threshold is equally too optimistic, as it requires crack growth of nearly 2 mm, by which time the residual strength is indeed rather poor (Fig. 8). Alternative approaches to design based on fatigue *R*-curves are the subject of ongoing work.[75]

The present results are in agreement with recent results on Si_3N_4,[53,76] where boundary strength was adjusted via sintering additives, and both steeper *R*-curves and higher sample strengths are being associated with stronger boundaries. Work on silicon carbide has also shown that changes in the interface chemistry and structure can cause a noticeable shift to more uncracked-ligament versus frictional bridging.[77] In this SiC family, both K_r, the nominal toughness, and the ΔK_{TH} threshold for long fatigue cracks, were greatest with more elastic bridging. Uncracked ligaments were argued to better resist fatigue loading as frictional wear is less effective for bridge degradation,[77] but concomitant microstructure changes (grain size, aspect ratio) make isolation of the various effects of interface chemistry/structure intractable. Although in that study the relative boundary strengths for each case were unknown, the present results indicate that such a shift to elastic bridging may reflect stronger boundaries.

Evidently, while sufficiently weak boundaries are essential for toughening via bridging in ceramics, it appears that the optimal window for boundary strength may be small. Indeed, if boundaries are weaker than optimal, the *R*-curves rise less steeply and fatigue is a larger problem due to the higher proportion of frictional bridging. Of course, it is also obvious that too much boundary strength leads to transgranular fracture and no extrinsic toughening, as is well illustrated for specific SiC- or Si_3N_4-based materials.[78–80]

V. Conclusions

Based on an experimental study on the role of moisture in affecting both the intrinsic and extrinsic factors governing the fracture and cyclic fatigue resistance of a polycrystalline alumina, several conclusions are made. It is noted that by changing the atmosphere to yield changes in the crack-tip resistance without changing the microstructure or residual stresses, new and unexpected insights into grain-bridging mechanisms have emerged.

1. Specifically, the presence of moisture was found definitively to lower the intrinsic toughness, K_0, of this alumina, as directly reflected by changes in transient crack-growth rates. Estimates based on crack-opening profiles show K_0 to be $\sim 30\%$ lower in moist relative to dry environments.

2. *R*-curves are initially much steeper in dry environments, indicating that more rapid development of significant bridging stresses ensues. This could lead to a factor of two or more larger strength for natural flaws in a dry atmosphere, a larger amount than would simply scale with the change in K_0.

3. For fatigue cracks between 20 and 60 μm long, where the role of crack bridging is diminished, growth rates are higher and fatigue thresholds significantly lower in moist air. However, this reduction in fatigue threshold with increased moisture content is larger than could be explained solely by differences in K_0. As with the *R*-curves, this was attributed to a difference in initial bridging contribution, specifically, in both cases, to a larger proportion of uncracked-ligament, as opposed to frictional, bridges in dry environments (consistent with the non-hysteretic compliance in dry N_2).

4. In contrast, for cracks many millimeters in length, moisture enhances the overall magnitude of bridging (K_{br}), apparently by promoting more frictional bridging under both monotonic fracture and fatigue conditions, resulting in similar *R*-curve and steady-state fatigue data for both environments. This is deemed to reflect competing effects, the moisture acting to lower the intrinsic toughness at the crack tip, but also to promote bridging in the crack wake.

5. The deduction of crack-tip toughnesses from crack-opening profiles allows estimation of nearly the entire *R*-curve. The deduced K_0 levels are below those for single crystals, consistent with the lower boundary toughnesses required to trigger bridging. In parallel, these K_0 values are so low that designing to absolute threshold to avoid initiation of any subcritical crack extension is much too conservative for these toughened materials, under either monotonic or cyclic loading. This is emphasized by the rapid decay in the fatigue growth of very short cracks, which, after arrest, should still have significant strength under subsequent monotonic loading.

6. These results indicate that there is an optimal boundary strength for promoting strength, fracture, and fatigue resistance. While excessively strong boundaries lead to transgranular cracking with neither bridging nor toughening, it appears that overly weak boundaries are also detrimental due to shallower *R*-curves, lower resultant strengths, and poorer fatigue resistance for short cracks.

Acknowledgments

The authors wish to thank Dr. Eric Stach and Doreen Ah Tye of the National Center for Electron Microscopy for aid in the *in situ* FESEM work and Rong Yuan for useful discussions.

References

[1]S. M. Wiederhorn, "Moisture Assisted Crack Growth in Ceramics," *Int. J. Fract. Mech.*, **4** [2] 171–77 (1968).
[2]A. G. Evans, "A Method for Evaluating the Time-Dependent Failure Characteristics of Brittle Materials—and its Application to Polycrystalline Alumina," *J. Mater. Sci*, **7**, 1137–46 (1972).
[3]S. M. Wiederhorn, B. J. Hockey, and D. E. Roberts, "Effect of Temperature on the Fracture of Sapphire," *Phil. Mag. A*, **28** [4] 783–96 (1973).
[4]S. W. Freiman, K. R. McKinney, and H. L. Smith, "Slow Crack Growth in Polycrystalline Ceramics;" pp. 659–76 in *Symposium of Fracture Mechanics of Ceramics*, Vol. 2. Edited by R. C. Bradt, D. P. H. Hasselmann, and F. F. Lange. Plenum New York, New York, 1974.
[5]M. E. Ebrahimi, J. Chevalier, and G. Fantozzi, "Slow Crack-Growth Behavior of Alumina Ceramics," *J. Mater. Res*, **15** [1] 142–7 (2000).
[6]A. H. De Aza, J. Chevalier, G. Fantozzi, M. Schehl, and R. Torrecillas, "Crack Growth Resistance of Alumina, Zirconia, and Zirconia Toughened Alumina Ceramics for Joint Prostheses," *Biomaterials*, **23** [3] 937–45 (2002).
[7]S. Lathabai and B. R. Lawn, "Fatigue Limits in Noncyclic Loading of Ceramics with Crack-Resistance Curves," *J. Mater. Sci.*, **24** [12] 4298–306 (1989).
[8]P. L. Swanson, C. J. Fairbanks, B. R. Lawn, Y.-W. Mai, and B. J. Hockey, "Crack-Interface Grain Bridging as a Fracture Resistance Mechanism in Ceramics: I, Experimental Study on Alumina," *J. Am. Ceram. Soc.*, **70** [4] 279–89 (1987).
[9]Y.-W. Mai and B. R. Lawn, "Crack-Interface Grain Bridging as a Fracture Resistance Mechanism in Ceramics: II, Theoretical Fracture Mechanics Model," *J. Am. Ceram. Soc.*, **70** [4] 289–94 (1987).
[10]R. M. McMeeking and A. G. Evans, "Mechanics of Transformation-Toughening in Brittle Materials," *J. Am. Ceram. Soc*, **65** [5] 242–6 (1982).
[11]A. G. Evans and R. M. Cannon, "Toughening of Brittle Solids by Martensitic Transformations," *Acta Metall.*, **34** [5] 761–800 (1986).
[12]R. O. Ritchie, "Mechanisms of Fatigue Crack Propagation in Metals, Ceramics and Composites: Role of Crack Tip Shielding," *Mater. Sci. Eng.*, **A103**, 15–28 (1988).
[13]S. M. Wiederhorn, "Influence of Water Vapor on Crack Propagation in Soda–Lime Glass," *J. Am. Ceram. Soc.*, **50** [8] 407–14 (1967).
[14]T. A. Michalske and S. W. Freiman, "A Molecular Mechanism for Stress Corrosion in Vitreous Silica," *J. Am. Ceram. Soc.*, **66** [4] 284–8 (1983).
[15]P. Chantikul, S. J. Bennison, and B. R. Lawn, "Role of Grain Size in the Strength and *R*-Curve Properties of Alumina," *J. Am. Ceram. Soc.*, **73** [8] 2419–27 (1990).
[16]S. J. Bennison and B. R. Lawn, "Role of Interfacial Grain-Bridging Sliding Friction in the Crack-Resistance and Strength Properties of Nontransforming Ceramics," *Acta Metall.*, **37** [10] 2659–71 (1989).

[17]R. M. Cannon, B. J. Dalgleish, and E. B. Slamovich, "Indentation Toughness of Polycrystalline Alumina," *Am. Ceram. Soc. Bull.*, **65** [3] 504 (1986).
[18]P. Gumbsch and R. M. Cannon, "Atomistic Aspects of Brittle Fracture," *Mater. Res. Soc. Bull.*, **25** [5] 15–20 (2000).
[19]M. D. Thouless, O. Sbaizero, L. S. Sigl, and A. G. Evans, "Effect of Interface Mechanical Properties on Pullout in a SiC-Fiber-Reinforced Lithium Aluminum Silicate Glass–Ceramic," *J. Am. Ceram. Soc.*, **72** [4] 525–32 (1989).
[20]P. F. Becher, C. H. Hsueh, K. B. Alexander, and E. Y. Sun, "Influence of Reinforcement Contact and Diameter on the *R*-Curve Response in SiC-Whisker-Reinforced Alumina," *J. Am. Ceram. Soc.*, **79** [2] 298–304 (1996).
[21]A. G. Evans, "High Toughness Ceramics," *Mater. Sci. Eng.*, **A105/6**, 65–75 (1988).
[22]R. O. Ritchie, "Mechanisms of Fatigue-Crack Propagation in Ductile and Brittle Solids," *Int. J. Fract*, **100** [1] 55–83 (1999).
[23]S. Lathabai, J. Rödel, and B. Lawn, "Cyclic Fatigue from Frictional Degradation at Bridging Grains in Alumina," *J. Am. Ceram. Soc*, **74** [6] 1348–60 (1991).
[24]C. J. Gilbert, R. N. Petrany, R. O. Ritchie, R. H. Dauskardt, and R. W. Steinbrech, "Cyclic Fatigue in Monolithic Alumina: Mechanisms for Crack Advance Promoted by Frictional Wear of Grain Bridges," *J. Mater. Sci*, **30** [3] 643–54 (1995).
[25]J. J. Kruzic, R. M. Cannon, and R. O. Ritchie, "Crack Size Effects on Cyclic and Monotonic Crack Growth in Polycrystalline Alumina: Quantification of the Role of Grain Bridging," *J. Am. Ceram. Soc*, **87** [1] 93–103 (2004).
[26]"ASTM E561-98," pp. 534–46 in *Annual Book of ASTM Standards, Vol. 03.01: Metals- Mechanical Testing; Elevated and Low-temperature Tests; Metallography*. ASTM, West Conshohocken, PA, USA, 2002.
[27]W. F. Deans and C. E. Richards, "A Simple and Sensitive Method of Monitoring Crack and Load in Compact Fracture Mechanics Specimens Using Strain Gages," *J. Test. Eval.*, **7** [3] 147–54 (1979).
[28]"ASTM E647-00," pp. 595–635 in *Annual Book of ASTM Standards, Vol. 03.01: Metals- Mechanical Testing; Elevated and Low-temperature Tests; Metallography*. ASTM, West Conshohocken, PA, USA, 2002.
[29]T. Fett, C. Mattheck, and D. Munz, "On the Calculation of Crack Opening Displacement From the Stress Intensity Factor," *Eng. Fract. Mech.*, **27**, 697–715 (1987).
[30]T. Fett, "Crack-Tip Toughness from Wide-Range COD Measurements," *Inter. J. Fract.*, **114** [4] L29–32 (2002).
[31]A. B. K. Njiwa, T. Fett, D. C. Lupascu, and J. Rödel, "Crack-Tip Toughness of a Soft Lead Zirconate Titanate," *J. Am. Ceram. Soc.*, **86** [11] 1973–5 (2003).
[32]T. Fett and D. Munz, *Stress Intensity Factors and Weight Functions*. Computational Mechanics Publications, Southampton, U.K., 1997.
[33]R. H. Dauskardt, "A Frictional-Wear Mechanism for Fatigue-Crack Growth in Grain Bridging Ceramics," *Acta Metall. Mater.*, **41** [9] 2765–81 (1993).
[34]R. D. Geraghty, J. C. Hay, and K. W. White, "Fatigue Degradation of the Crack Wake Zone in Monolithic Alumina," *Acta Mater.*, **47** [4] 1345–53 (1999).
[35]M. Iwasa and R. C. Bradt, "The Fracture Toughness of Single Crystal Alumina;" pp. 767–79 in Advances in Ceramics, Vol. 10, *Structure and Properties of MgO and Al_2O_3 Ceramics*, Edited by W. D. Kingery. American Ceramic Society, Columbus, OH, 1984.
[36]P. F. Becher, "Fracture-Strength Anisotropy of Sapphire," *J. Am. Ceram. Soc.*, **59** [1–2] 59–61 (1976).
[37]S. M. Wiederhorn, "Fracture of Sapphire," *J. Am. Ceram. Soc.*, **52** [9] 485–91 (1969).
[38]E. B. Shand, "Correlation of Strength of Glass with Fracture Flaws of Measured Size," *J. Am. Ceram. Soc.*, **44** [9] 451–5 (1961).
[39]S. M. Wiederhorn, "Fracture Surface Energy of Glass," *J. Am. Ceram. Soc.*, **52** [2] 99–105 (1969).
[40]J. Nakayama, "Direct Measurement of Fracture Energies of Brittle Heterogeneous Materials," *J. Am. Ceram. Soc.*, **48** [11] 583–7 (1965).
[41]R. W. Davidge and G. Tappin, "The Effective Surface Energy of Brittle Materials," *J. Mater. Sci.*, **3** [2] 165–73 (1968).
[42]S. M. Wiederhorn and L. H. Bolz, "Stress Corrosion and Static Fatigue of Glass," *J. Am. Ceram. Soc.*, **53** [10] 543–48 (1970).
[43]S. M. Wiederhorn, S. W. Freiman, E. R. Fuller, and C. J. Simmons, "Effects of Water and other Dielectrics on Crack Growth," *J. Mater. Sci.*, **17** [12] 3460–78 (1982).
[44]M.-Y. He and J. W. Hutchinson, "Crack Deflection at an Interface Between Dissimilar Elastic Materials," *Inter. J. Solids Struct.*, **25** [9] 1053–67 (1989).
[45]J. Seidel and J. Rödel, "Measurement of Crack Tip Toughness in Alumina as a Function of Grain Size," *J. Am. Ceram. Soc.*, **80** [2] 433–38 (1997).
[46]J. Rödel, J. F. Kelly, and B. R. Lawn, "*In situ* Measurements of Bridged Crack Interfaces in the Scanning Electron Microscope," *J. Am. Ceram. Soc.*, **73** [11] 3313–18 (1990).
[47]T. Fett, D. Munz, J. Seidel, M. Stech, and J. Rödel, "Correlation Between Long and Short Crack *R*-Curves in Alumina Using the Crack Opening Displacement and Fracture Mechanical Weight Function Approach," *J. Am. Ceram. Soc.*, **79** [5] 1189–96 (1996).
[48]O. Raddatz, G. A. Schneider, and N. Claussen, "Modeling of *R*-Curve Behavior in Ceramic/Metal Composites," *Acta Mater.*, **46** [18] 6381–95 (1998).
[49]O. Raddatz, G. A. Schneider, W. Mackens, H. Voss, and N. Claussen, "Bridging Stresses and *R*-curves in Ceramic/Metal Composites," *J. Eur. Ceram. Soc.*, **20** [13] 2261–73 (2000).
[50]J. J. Kruzic, R. A. Marks, M. Yoshiya, A. M. Glaeser, R. M. Cannon, and R. O. Ritchie, "Fracture and Fatigue Behavior at Ambient and Elevated Temperatures of Alumina Bonded with Copper/Niobium/Copper Interlayers," *J. Am. Ceram. Soc.*, **85** [10] 2531–41 (2002).
[51]R. F. Cook and A. G. Schrott, "Calcium Segregation to Grain Boundaries in Alumina," *J. Am. Ceram. Soc.*, **71** [1] 50–58 (1988).
[52]W. R. Cannon and E. A. Mendoza, "Measurement of K_{tip} in Fiber and Whisker Composites;" pp. 735–42 in *Proceedings of the 4th International Symposium on Ceramic Materials and Components for Heat Engines*, Edited by R. Carlsson, T. Johansson, and L. Kahlman. Elsevier Applied Science, London, U.K., 1992.
[53]R. L. Satet, J. J. Kruzic, M. J. Hoffmann, R. M. Cannon, and R. O. Ritchie, "Relations of Strength, Fracture Toughness and Grain Boundary Strength in Rare Earth-Doped Si_3N_4–Ceramics," *J. Am. Ceram. Soc.*, (2005) to be submitted.
[54]J. Rödel, "Crack Closure Forces in Ceramics: Characterization and Formation," *J. Eur. Ceram. Soc*, **9** [4] 323–34 (1992).
[55]G. Pezzotti, O. Sbaizero, V. Sergo, N. Muraki, K. Maruyama, and T. Nishida, "*In situ* Measurements of Frictional Bridging Stresses in Alumina Using Fluorescence Spectroscopy," *J. Am. Ceram. Soc*, **81** [1] 187–92 (1998).
[56]G. Pezzotti, N. Muraki, N. Maeda, K. Satou, and T. Nishida, "*In situ* Measurement of Bridging Stresses in Toughened Silicon Nitride Using Raman Microprobe Spectroscopy," *J. Am. Ceram. Soc*, **82** [5] 1249–56 (1999).
[57]D. K. Tran, A. S. Kobayashi, and K. W. White, "Crack Growth in Alumina at High Temperature," *Eng. Fract. Mech*, **68** [2] 149–61 (2001).
[58]P. Andersson, "Pin-On-Disk Tests With Ceramics in Air and Aqueous Media;" pp. 1241–47 in *Proceedings of the 4th International Symposium on Ceramic Materials and Components for Heat Engines*, Edited by R. Carlsson, T. Johansson, and L. Kahlman. Elsevier Applied Science, London, U.K., 1992.
[59]A. Kahn, H. M. Chan, M. P. Harmer, and R. F. Cook, "Toughening of an Alumina–Mullite Composite by Unbroken Bridging Elements," *J. Am. Ceram. Soc*, **83** [4] 833–40 (2000).
[60]F. A. McClintock, "A Three-Dimensional Model for Polycrystalline Cleavage and Problems in Cleavage After Extended Plastic Flow or Cracking;" pp. 81–94 in *Cleavage Fracture: George R. Irwin Symposium*, Edited by K. S. Chan. TMS, Warrendale, PA, 1997.
[61]Y. Qiao, "Modeling of Resistance Curve of High-Angle Grain Boundary in Fe–3wt%Si Alloy," *Mater. Sci. Eng.*, **A361** [1–2] 350–57 (2003).
[62]Y. Qiao and A. S. Argon, "Cleavage Cracking Resistance of High Angle Grain Boundaries in Fe–3%Si Alloy," *Mech. Mater.*, **36** [3–6] 313–31 (2003).
[63]T. J. Becker Jr., R. M. Cannon, and R. O. Ritchie, "Statistical Fracture Modeling: Crack Path and Fracture Criteria with Application to Homogeneous and Functionally Graded Materials," *Eng. Fract. Mech.*, **69** [14–16] 1521–55 (2002).
[64]A. Bhatnagar, M. J. Hoffmann, and R. H. Dauskardt, "Fracture and Subcritical Crack-Growth Behavior of Y–Si–Al–O–N Glasses and Si_3N_4 Ceramics," *J. Am. Ceram. Soc.*, **83** [3] 585–96 (2000).
[65]D. S. Jacobs and I.-W. Chen, "Mechanical and Environmental Factors in the Cyclic and Static Fatigue of Silicon Nitride," *J. Am. Ceram. Soc.*, **77** [5] 1153–61 (1994).
[66]R. Steinbrech, R. Knehans, and W. Schaawächter, "Increase of Crack Resistance During Slow Crack Growth in Al_2O_3 Bend Specimens," *J. Mater. Sci.*, **18**, 265–70 (1983).
[67]K.-S. Sohn, S. Lee, and S. Baik, "Analytical Modeling for Bridging Stress Function Involving Grain Size Distribution in a Polycrystalline Alumina," *J. Am. Ceram. Soc.*, **78** [5] 1401–5 (1995).
[68]S. Kovalev, T. Miyajima, Y. Yamauchi, and M. Sakai, "Numerical Evaluation of Toughening by Crack-Face Grain Interlocking in Self-Reinforced Ceramics," *J. Am. Ceram. Soc.*, **83** [4] 817–24 (2000).
[69]S. Kovalev, T. Miyajima, and Y. Yamauchi, "Micromechanics of Crack Bridging by Elongated Crystals in Self-Reinforced Ceramic Materials," *Key Eng. Mater.*, **161–3**, 615–8 (1999).
[70]G. K. Bansal, W. H. Duckworth, and D. E. Niesz, "Strength-Size Relations in Ceramic Materials: Investigation of an Alumina Ceramic," *J. Am. Ceram. Soc.*, **59** [11–12] 472–8 (1976).
[71]S.-J. Cho, K.-J. Yoon, J.-J. Kim, and K.-H. Kim, "Influence of Humidity on the Flexural Strength of Alumina," *J. Eur. Ceram. Soc.*, **20** [6] 761–4 (2000).
[72]S.-J. Cho, K.-J. Yoon, Y.-C. Lee, and M.-C. Chu, "Effects of Environmental Temperature and Humidity on the Flexural Strength of Alumina and Measurement of Environment-Insensitive Inherent Strength," *Mater. Lett.*, **57** [18] 2751–4 (2003).
[73]C. C. McMahon, "Relative Humidity and Modulus of Rupture," *Am. Ceram. Soc. Bull.*, **58** [9] 873 (1979).
[74]B. Pletka and S. M. Wiederhorn, "Subcritical Crack Growth in Glass Ceramics;" pp. 745–60 in *Fracture Mechanics of Ceramics*, Vol. 4. Edited by R. C. Bradt, D. P. H. Hasselman, and F. F. Lange. Plenum Press, New York, 1978.
[75]J. J. Kruzic, R. M. Cannon, J. W. Ager III, and R. O. Ritchie, "Fatigue Threshold *R*-Curves For Predicting Reliability of Ceramics Under Cyclic Loading," *Acta Mater.*, **53** [9] 2595–605 (2005).
[76]R. L. Satet and M. J. Hoffmann, "Influence of the Grain Boundary Phase Chemistry on the Mechanical Properties of Silicon Nitride," *J. Am. Ceram. Soc.*, (2005) in press.
[77]R. Yuan, J. J. Kruzic, X. F. Zhang, L. C. De Jonghe, and R. O. Ritchie, "Ambient to High-Temperature Fracture Toughness and Cyclic Fatigue Behavior in Al-Containing Silicon Carbide Ceramics," *Acta Mater.*, **51** [20] 6477–91 (2003).
[78]C. J. Gilbert, J. J. Cao, L. C. De Jonghe, and R. O. Ritchie, "Crack-Growth Resistance-Curve Behavior in Silicon Carbide: Small Versus Long Cracks," *J. Am. Ceram. Soc.*, **80** [9] 2253–61 (1997).
[79]M. J. Hoffmann, A. Geyer, and R. Oberacker, "Potential of the Sinter-HIP-Technique for the Development of High-Temperature Resistance Si_3N_4–Ceramics," *J. Eur. Ceram. Soc.*, **19** [13–14] 2359–66 (1999).
[80]G. Pezzotti, I. Tanaka, and T. Nishida, "Intrinsic Fracture Energy of Polycrystalline Silicon Nitride," *Phil. Mag. Lett.*, **65**, 95–100 (1993). □